Neuron, Vol. 47, 423–435, August 4, 2005, Copyright ©2005 by Elsevier Inc. DOI 10.1016/j.neuron.2005.06.016

Inhibitory Postsynaptic Potentials Carry Synchronized Frequency Information in Active Cortical Networks

Andrea Hasenstaub, Yousheng Shu, Bilal Haider, Udo Kraushaar,[1] Alvaro Duque, and David A. McCormick*
Department of Neurobiology
Kavli Institute of Neuroscience
Yale University School of Medicine
333 Cedar Street
New Haven, Connecticut 06510

Summary

Temporal precision in spike timing is important in cortical function, interactions, and plasticity. We found that, during periods of recurrent network activity (UP states), cortical pyramidal cells in vivo and in vitro receive strong barrages of both excitatory and inhibitory postsynaptic potentials, with the inhibitory potentials showing much higher power at all frequencies above approximately 10 Hz and more synchrony between nearby neurons. Fast-spiking inhibitory interneurons discharged strongly in relation to higher-frequency oscillations in the field potential in vivo and possess membrane, synaptic, and action potential properties that are advantageous for transmission of higher-frequency activity. Intracellular injection of synaptic conductances having the characteristics of the recorded EPSPs and IPSPs reveal that IPSPs are important in controlling the timing and probability of action potential generation in pyramidal cells. Our results support the hypothesis that inhibitory networks are largely responsible for the dissemination of higher-frequency activity in cortex.

Introduction

The encoding of information in cortical networks depends not only upon the rate at which action potentials are generated by individual cells, but also on the temporal precision and the relative timing of action potentials between neurons in an interacting network (Foffani et al., 2004; Lu et al., 2001; Singer and Gray, 1995). Intracellular investigations of the spike-generating mechanism in cortical neurons indicate that it is capable of precision in the submillisecond range, given a synaptic input that contains high-frequency components (Mainen and Sejnowski, 1995; Nowak et al., 1997). Cortical networks generate activity at a broad range of frequencies, from well below one up to hundreds of hertz (Buzsaki and Draguhn, 2004; Jones et al., 2000; Steriade, 1997). Although the cellular mechanisms for generation of slow, sleep-related neocortical oscillations have been detailed (reviewed in Steriade, 1997; Steriade et al., 1993a), generation of higher frequencies in neocortical networks in vivo has remained largely unexplored. Of particular interest is the generation of gamma band (30–80 Hz) activity, since this is often associated with an activated cortical network. In vivo and in vitro recordings in the hippocampus indicate that the discharge of inhibitory neurons plays a key role in higher-frequency network activities (Csicsvari et al., 2003; Penttonen et al., 1998; Whittington et al., 1995; reviewed in Buzsaki and Chrobak, 1995; Jonas et al., 2004). These interneurons may discharge synchronously either through a coordinated drive from pyramidal cells or their axons (Csicsvari et al., 2003; Mann et al., 2005; Traub et al., 2004), or through the effects of interneuronal gap junction and/or synaptic interactions (Deans et al., 2001; Galarreta and Hestrin, 1999; Gibson et al., 2005). In the neocortex, it has been proposed that a specialized subgroup of pyramidal cells, chattering neurons (Cunningham et al., 2004; Gray and McCormick, 1996), are critically involved in the generation of gamma frequency network oscillations, although in vitro results suggest an important role for inhibitory neurons in this, and lower-frequency, synchronized activities (Deans et al., 2001; Gibson et al., 2005).

An important role for inhibition in precise spike timing and higher-frequency activity is suggested by a standard feature of cortical networks: excitatory afferents typically contact not only pyramidal cells, but also GABAergic neurons, resulting in monosynaptic excitation followed after a short interval by disynaptic inhibition in the recipient pyramidal cell, effectively "sharpening" the characteristics of synaptic inputs (Pouille and Scanziani, 2001; Wehr and Zador, 2003). Fast-spiking (FS) GABAergic neurons such as basket cells innervate the cell body and proximal dendrites of pyramidal cells, while chandelier cells innervate the axon initial segment of pyramidal cells; both are preferred locations for controlling the timing and probability of action potential generation in pyramidal cells (Cobb et al., 1995; Miles et al., 1996; Pouille and Scanziani, 2001). The presence of electrotonic coupling through gap junctions between cortical GABAergic neurons (Galarreta and Hestrin, 1999; Galarreta and Hestrin, 2002; Gibson et al., 1999; Hormuzdi et al., 2001) suggests that these cells may generate large, synchronous inhibitory potentials within cortical networks.

Here, using the spontaneously occurring recurrent network activity in vivo and in vitro of the so-called UP and DOWN states, we demonstrate that inhibitory synaptic potentials carry the large majority of power in the frequency range of 10–100 Hz and indeed often synchronously inhibit nearby pyramidal cells. These results support the hypothesis that GABAergic interneurons are critical in determining temporal coding and spike timing precision in cortical networks.

Results

Loss of Inhibition Abolishes Higher Frequencies in Spontaneous Network Activity

Intracellular, extracellular multiple-unit, and field potential recordings in the dorsal prefrontal cortex of either

*Correspondence: david.mccormick@yale.edu
[1]Present address: Institute for Molecular Cell Biology, Building 61, Saarland University, D-66421 Homburg, Germany.

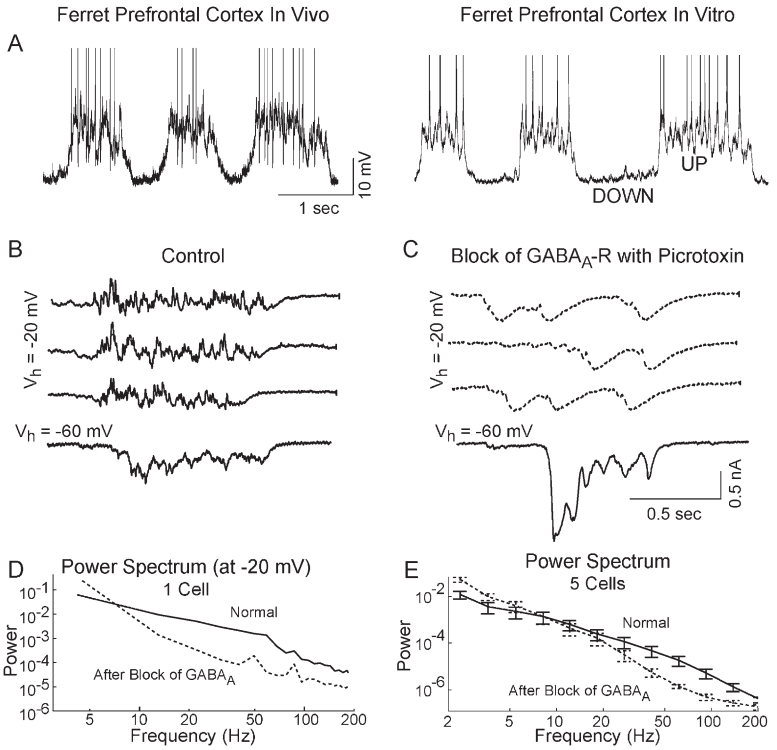

Figure 1. Membrane Potential during Periods of Recurrent Synaptic Activity Contains a Broad Range of Frequencies, and the Higher Frequencies Are Selectively Attenuated by Block of $GABA_A$ Receptors

(A) Intracellular recordings (KAc-filled microelectrodes) of UP and DOWN states in vivo (left) and in vitro (right) showing the typical pattern of depolarization, action potential activation, and synaptic barrages associated with recurrent activity. (B) Three consecutive examples of synaptic currents arriving in a layer 5 pyramidal cell in vitro while voltage clamped near the reversal potential of the UP state (–20 mV in this cell) and one trace at –60 mV. (C) Local application of picrotoxin (PTX) results in a marked decrease in the higher-frequency components of the synaptic currents, prior to the generation of epileptiform bursts. (D) Power spectra of the PSCs in (B) and (C). The reduction of $GABA_A$ receptor-mediated inhibition resulted in an increase in power below 10 Hz, and a decrease in power above 10 Hz. (E) Power spectra (near reversal potential) of PSCs pre- and post-PTX in n = 5 cells. After reduction of $GABA_A$ receptor-mediated inhibitory synaptic transmission, there was significantly more power at frequencies below 5 Hz and significantly less power at frequencies above 35 Hz. All data, except for that in (A), left, were collected from RS neurons in the interface chamber in vitro with sharp electrodes. In (B)–(E), microelectrodes contained QX-314 and CsAc. Error bars represent standard error of the mean.

ketamine/xylazine-anesthetized ferrets or in layer 5 of a ferret prefrontal cortical slice maintained in vitro exhibited robust and spontaneous UP and DOWN states (Figure 1A). The UP state is characterized by the arrival of large barrages of postsynaptic potentials, which depolarize the neuron by 5–25 mV in vivo (n = 30 cells) and 5–15 mV in vitro (n = 55 cells). The UP state causes regular-spiking (RS) cells to discharge at approximately 3–30 Hz, both in vivo and in vitro (Figure 1A). In between UP states, the membrane potential is relatively hyperpolarized, and there is a marked decrease in synaptic activity (Cowan and Wilson, 1994; Shu et al., 2003a; Shu et al., 2003b; Steriade et al., 1993b; Steriade et al., 2001). The UP state is generated through local recurrent excitation that is balanced and controlled by the activity of GABAergic interneurons (Sanchez-Vives and McCormick, 2000; Shu et al., 2003b).

To examine the properties of the synaptic inputs arriving in the UP state, we moved the membrane potential to different levels with either the intracellular injection of direct current (current-clamp mode) or through the application of single-electrode voltage clamp, both in vivo and in vitro (Figure 1B). To examine the properties of incoming synaptic currents, we typically included 50 mM QX-314 and 2 M CsAc in our sharp intracellular pipettes to reduce Na^+, K^+, and other intrinsic currents. The results obtained either in anesthetized ferrets or in slices in vitro were similar (except where stated). We have previously reported that the synaptic activity arriving in cortical pyramidal cells during the UP state in vitro is a proportional mixture of excitatory and inhibitory potentials that exhibits a net reversal potential of between –20 and –40 mV (Shu et al., 2003b). Examination of the synaptic potentials or synaptic currents arriving in these cells, either at membrane potentials near the reversal potential of the synaptic barrages (–20 to –40 mV), or at membrane potentials near those of the UP state (–55 to –60 mV), revealed a broad range of frequencies in the power spectrum (Figure 1B; n = 6). The block of $GABA_A$ receptors with local application of picrotoxin (50 μM in micropipette) rapidly resulted in an elevation of power at low (<10 Hz) frequencies and greatly reduced power at higher frequencies (Figures 1C–1E; n = 6), well before the appearance of epileptiform activity (Sanchez-Vives and McCormick, 2000). This result indicates that the proper functioning of $GABA_A$ receptor-mediated inhibitory systems in the neocortex is required for the generation of higher frequencies in network-driven synaptic barrages.

Inhibitory Synaptic Barrages Contain More Power at Higher Frequencies

A general block of inhibition results in large changes in network behavior, eventually leading to the generation of epileptiform activity. To isolate the properties of excitatory or inhibitory synaptic inputs without affecting network activity, we controlled the membrane potential of the recorded cell through the intracellular injection of current (either in current or voltage clamp) such that the UP state occurred either at the reversal potential of

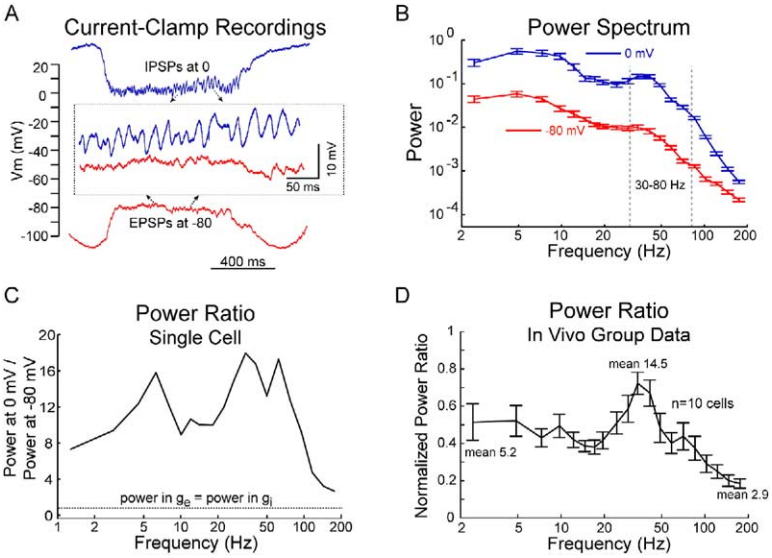

Figure 2. Comparison of the Power of the Membrane Potential at Voltages Where It Is Dominated by Either Excitatory or Inhibitory Synaptic Inputs during the UP State In Vivo

(A) Intracellular recordings in ferret prefrontal cortex illustrating the amplitude and time course of excitation-dominated synaptic barrages recorded at –80 mV (red) and inhibition-dominated barrages recorded at 0 mV (blue), for two representative UP states. Membrane potentials are expanded further for illustration (inset). (B) Power spectra of multiple UP states for the cell in (A) demonstrating that IPSPs contain more power at all frequencies above approximately 2 Hz. (C) The ratio of average power in the inhibition-dominated and excitation-dominated barrages shows that the IPSPs are not simply scaled versions of the EPSPs. (D) Normalized ratio of power in IPSPs to power in EPSPs in ten cells. The peak ratio in each cell was normalized to a value of 1. The average nonnormalized ratio at the peak was 14.5 ± 9 (standard deviation). Data were collected from RS neurons in vivo with sharp electrodes containing QX-314 and CsAc. Error bars represent standard error of the mean.

EPSCs (0 mV; to examine IPSCs in relative isolation) or at the reversal potential for IPSCs (–75 to –80 mV; to examine EPSCs) (see Figure 2). Although these synaptic barrages will not be purely excitatory or inhibitory (due to incomplete voltage or space clamp, for example), at these membrane potentials they will be dominated by one or the other (Shu et al., 2003b).

Results obtained in vivo or in vitro were similar unless otherwise stated. During the UP state, synaptic barrages dominated by excitation (recorded near –80 mV) exhibited smoother membrane potential deflections than did synaptic barrages dominated by inhibition (recorded near 0 mV) (Figure 2A; n = 10 in vivo; n = 6 in vitro). Examination of power versus frequency for segments of UP states recorded at 0 and –80 mV revealed that both IPSP/C and EPSP/C barrages exhibited a progressive decrease in power with increase in frequency, although the power in the IPSP/C barrages was significantly higher than that in the EPSP/C barrages in the frequency range of 2 to 102 Hz (Figure 2B). Often, particularly for in vivo recordings, the IPSP/IPSC barrages exhibited more power at the 30–80 Hz (gamma frequency) range than would be expected, given the steady falloff of power with frequency (Figure 2B). Excitatory PSPs/PSCs either exhibited a smaller (n = 5/10) or no evident (n = 5/10) enhancement of gamma frequency power. In individual cells (e.g., Figures 2C and 2D), plots of the ratio of power in IPSP/Cs versus EPSP/Cs arriving in the same neurons during UP states often revealed a progressive increase between the frequencies of approximately 1–10 Hz followed by a progressive decrease above approximately 60–80 Hz. In between 10 and 80 Hz, the ratio typically exhibited one or two and sometimes three peaks at frequencies between 20 and approximately 70 Hz (Figure 2C). Although the precise location of these peaks varied between recorded cells, group averages of the normalized ratio of power in IPSPs versus EPSPs revealed a gradual increase and decrease, with the peak ratio centered around 40 Hz (Figure 2D). At this peak, there was 14.5 ± 9 times as much power in the IPSPs as EPSPs, while at 2 Hz the ratio was 5.2 ± 1.8, and at 200 Hz it dropped to 2.9 ± 1.5.

Differences between UP State Synaptic Barrages in FS Inhibitory Interneurons and RS Pyramidal Cells

We hypothesized that FS neurons, a major GABAergic cell type in the cortex (Kawaguchi, 1995; McCormick et al., 1985; Nowak et al., 2003), may possess specific membrane and synaptic properties that allow them to convey a broad frequency range of activity in cortical networks. Indeed, the barrages of PSPs arriving in FS GABAergic cells in vitro at –70 to –60 mV during the UP state appeared to be dominated by briefer and "sharper" events than those arriving in RS pyramidal neurons (Figure 3; n = 21 RS cells; n = 11 FS cells). Examination of the power spectra of the PSP barrages revealed that FS cells have progressively more power than RS cells at frequencies above approximately 25–30 Hz (see Figures 3E and 3F; n = 8 RS; n = 7 FS cells). Part of these differences may be the result of the shorter membrane time constant of FS cells in comparison to RS neurons, resulting in less attenuation of higher frequencies in FS neurons (sharp electrodes and fit with a single exponential function; FS cells: 4.3 ± 1.2 ms, n = 8; RS cells: 14.7 ± 7.2 ms, n = 13) (McCormick et al., 1985; Nowak et al., 2003). To test this hypothesis, we injected, through a dynamic-clamp system (Shu et al., 2003a), colored conductance noise while recording from physiologically identified FS and RS neurons with the whole-cell patch-clamp technique in vitro (see Experimental Procedures) and examined the resulting deviation in membrane potential (Figures 4A–4C; n = 21 RS cells; n = 11 FS cells; membrane time constants for

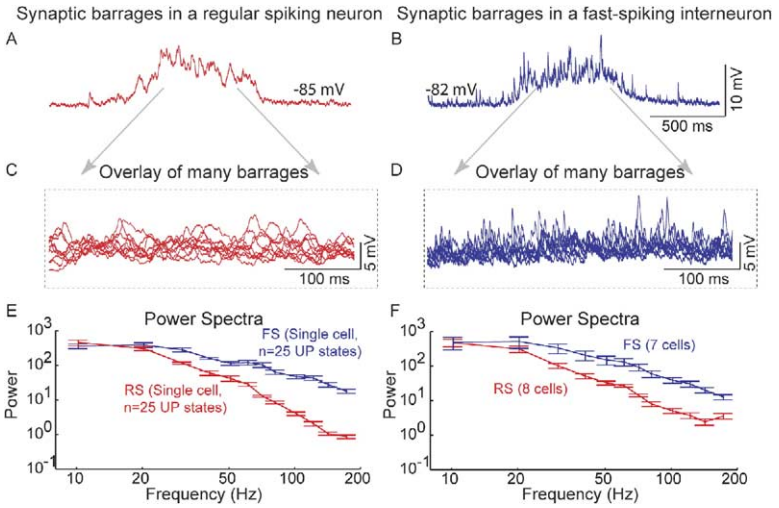

Figure 3. Barrages of PSPs Arriving in FS Inhibitory Interneurons Contain More Power at Higher Frequencies Than the Comparable Barrages in RS Pyramidal Neurons

Examples of synaptic barrages in a layer 5 RS pyramidal neuron in vitro (A and C) and a FS inhibitory interneuron in vitro (B and D). (E) The synaptic barrages in FS interneurons contain more power at frequencies above 20 Hz than those in RS pyramidal cells. (F) Group data. All data were collected from layer 5 neurons in the interface chamber with sharp electrodes containing Kac; all cells were slightly hyperpolarized through intracellular current injection to prevent action potential generation. Error bars represent standard error of the mean.

the two cell types in whole-cell recordings were 28.4 ± 12.2 and 12.0 ± 4.8, respectively). The calculation of the power transfer between conductance injected and voltage fluctuations revealed that, although both cell types exhibited a decrease in membrane potential deviation with increase in frequency, this decrease was greater for RS than FS cells above approximately 12 Hz (Figure 4C). Likewise, examining the representation of different frequencies in the action potential output of cortical cells in response to the intracellular injection of colored noise (see Experimental Procedures) revealed that RS neurons (n = 16) showed resonance at 5 to 10 Hz and attenuation at higher frequencies, while FS neurons (n = 8) showed greater representation of inputs at frequencies above 15 Hz (Figure 4F). Interestingly, in many FS interneurons (n = 6/8) the transfer of frequencies in the spike train peaked near gamma frequencies, 30–80 Hz (Figure 4F).

Action Potential Refractory Period in FS Neurons Is Shorter Than that in RS Cells

Measuring the spike refractory period for FS neurons revealed that it lasted, on average, only 32 ± 12 ms (see the Supplemental Data available with this article online; n = 8), which is significantly shorter than that found in RS pyramidal cells in vitro (90 ± 8.9 ms; n = 11; $p < 0.001$) (Shu et al., 2003a). This difference in spike refractory periods presumably contributes strongly to the

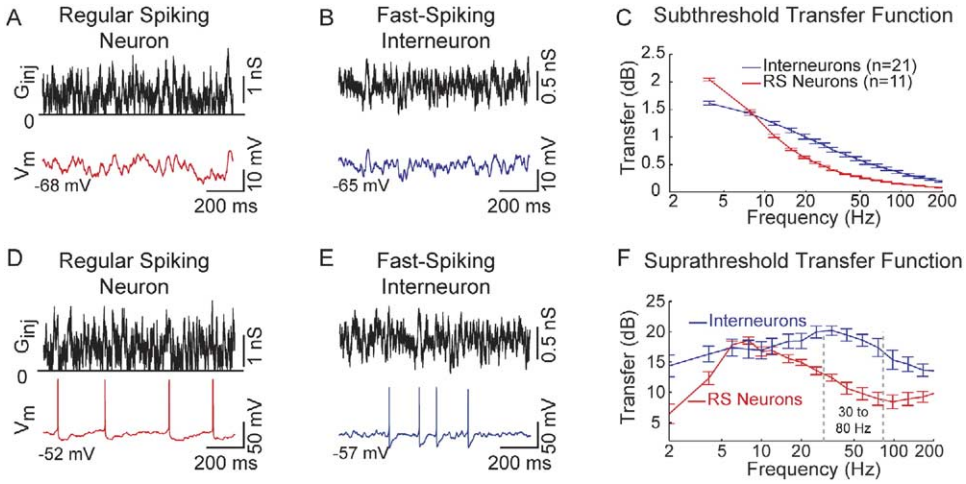

Figure 4. FS GABAergic Neurons, Compared to RS Principal Neurons, Exhibit Membrane Properties that Cause Less High-Frequency Attenuation

Examples of the membrane response of a pyramidal cell (A) and a FS GABAergic cell (B) to the injection of conductance noise. (C) Transfer functions (output power/input power) showing that FS neurons transfer more power at almost all frequencies above 10 Hz (n = 21 FS and 11 RS cells). (D) Example of the spiking response of a pyramidal cell to the injection of noise. (E) Example of the spiking response of a FS GABAergic cell to the intracellular injection of similar noise. (F) Transfer function of the injected current to spike times for the RS (n = 16) and FS (n = 8) neurons. Data were collected from RS and FS neurons in a submerged slice in vitro with whole-cell patch-clamp recordings. Error bars represent standard error of the mean.

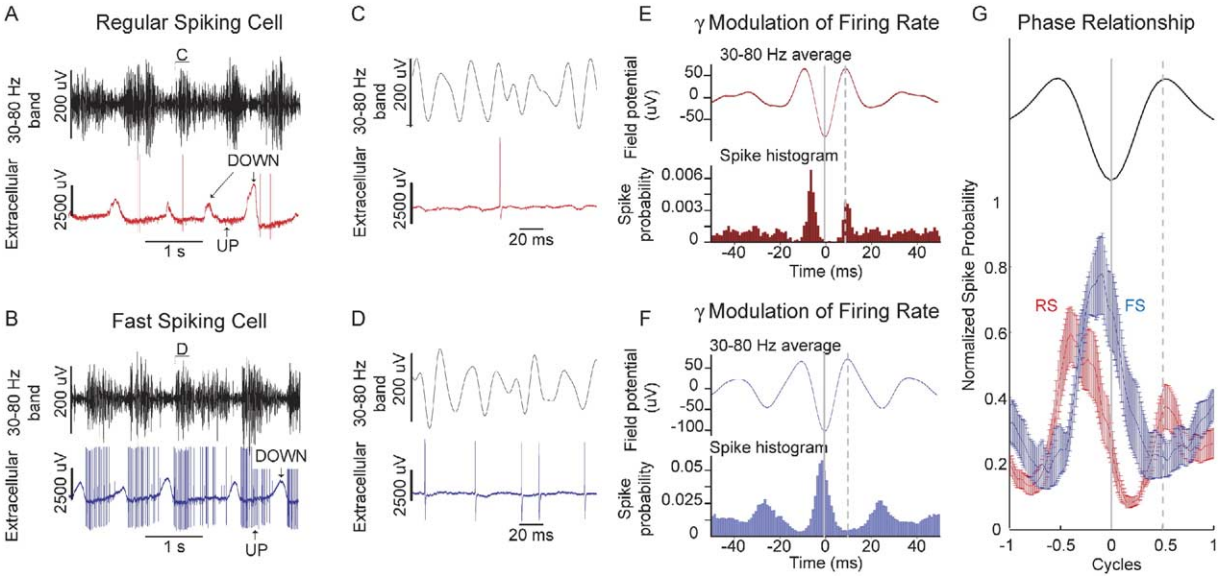

Figure 5. Both RS and FS Neurons Fire in Phase with Gamma Frequency Field Activity

(A and B) Extracellular broadband and gamma-filtered recording of a RS cell (A) and a FS interneuron (B). The lower trace in each case is the broadband, unfiltered recording, while the upper trace is the same recording filtered at 30–80 Hz to demonstrate the gamma band frequencies in the field potential. (C and D) Expansion of traces shows that the RS cell discharges just before the trough of gamma activity, while the FS cell fires closer to the gamma band trough. (E and F) Waveform averages of the gamma band synced on gamma trough (top) and trough-triggered averages of the extracellularly recorded spikes. (G) Averages (widths normalized to the period of the extracellular gamma oscillation) of the normalized (peak probability = 1) FS (n = 7 cells) and RS (n = 14 cells) cell firing probabilities. Error bars represent standard error of the mean.

preferred firing frequency of these two types of neurons in response to noise injection (see Supplemental Data).

FS and RS Cells Discharge Differentially in Relation to 30–80 Hz Oscillations in the Local Field Potential In Vivo

To test the hypothesis that inhibitory neurons in the neocortex play an important role in the generation of higher-frequency activities in local networks, we recorded extracellularly from single neurons in the ferret prefrontal cortex in vivo, identified these cells as either RS or FS (see Experimental Procedures and Supplemental Data), and correlated their activity with the gamma band oscillations of the local field potential recorded from the same electrode (Figure 5). Extracellular recordings revealed FS cells (n = 7) to discharge strongly (mean rate of 10–35 Hz; see Supplemental Data) during UP states (Figure 5B and Figure S4), while RS cells discharged at a lower mean rate of 0.5 to 15 Hz (Figure 5A; see Supplemental Data). Filtering the field potential for gamma frequencies (30–80 Hz) isolated the prominent gamma oscillation in the local field potential (mean frequency of 44–68 Hz; n = 22 recordings). Plotting a perievent histogram of FS and RS cell discharge synchronized on the trough of the gamma field potential oscillation revealed a strong relationship between the probability of discharge in both FS and RS cells and the phase of the gamma oscillation in the local field potential (Figures 5E and 5F). RS activity peaked at a phase of –0.26 cycles (±0.14; n = 14; 0 = gamma trough, 0.5 = gamma peak), while FS interneurons discharged on average at a phase of –0.03 (±0.17; Figure 5G), indicating that RS cells on average lead FS cell discharge by 4.1 ms (FS cells fire at –1.0 ± 3.0 ms; RS cells fire at –5.1 ± 2.4 ms; $p < 0.01$).

Modulation of Membrane Potential in Relation to 30–80 Hz Oscillations in the Local Field

Simultaneous extracellular field potential and nearby (within 0.8 mm) intracellular recordings from RS cells (n = 9) were performed while the membrane potential of the RS cells was depolarized and hyperpolarized to various levels with the intracellular injection of current (Figures 6A–6D; QX-314 and Cs^+ included in the micropipette). Filtering the field potential for 30–80 Hz activity, and then performing a field potential trough-triggered average of the intracellularly recorded membrane potential at either near –80 mV or 0 mV (Figures 6E and 6F) revealed that both excitation-dominated barrages and inhibition-dominated barrages are modulated in relation to gamma oscillations in the local field; however, inhibition-dominated barrages are more strongly modulated (mean peak-to-trough height 1.8 ± 0.8 mV, compared to 0.9 ± 0.4 mV for excitation-dominated barrages; mean difference of 0.8 ± 0.6 mV; $p < 0.05$, Wilcoxon sign rank test).

Barrages of IPSPs, but Not EPSPs, Show Marked Synchrony between Simultaneously Recorded RS Neurons

To examine the possibility that inhibitory potentials may exhibit a higher degree of synchrony than excitatory

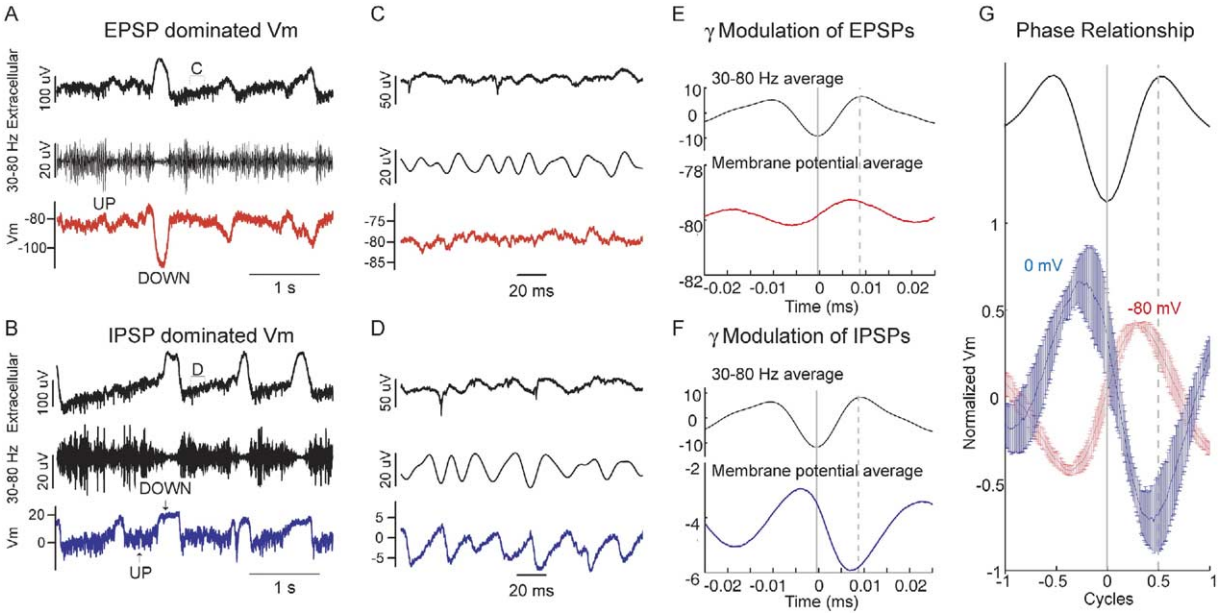

Figure 6. IPSP- and EPSP-Dominated Synaptic Barrages Are Modulated in Phase with Gamma Field Potential Activity In Vivo

(A and B) Extracellular broadband, gamma-filtered broadband, and intracellular recordings of a RS neuron. (C and D) Expansion of traces shows weak relationship between gamma-filtered broadband and EPSP-dominated membrane potentials, while gamma-filtered broadband and IPSP-dominated traces are more strongly related. (E and F) Gamma trough-triggered averages of gamma-filtered broadband (top) and intracellular membrane potential (bottom) show stronger modulation of IPSP- than EPSP-dominated membrane potential by gamma. (G) Averages (widths normalized to period of extracellular gamma oscillation) of the normalized (IPSP peak-to-peak deviation = 2; mean = 0) IPSPs and EPSPs for n = 9 cells show that IPSPs are more modulated by gamma than are EPSPs and show the EPSP peak slightly preceding the IPSP trough. Intracellular electrodes contained QX-314 and CsAc. Error bars represent standard error of the mean.

potentials during the UP state, we intracellularly recorded (sharp electrodes) simultaneously from pairs of nearby RS pyramidal neurons in vitro (within 100 μm) and in vivo (pairs within 1.2 mm; see Supplemental Data). In vitro (Figures 7A, 7C, and 7D), the inhibition-dominated barrages recorded simultaneously from neighboring cells (both held near 0 mV) showed a higher cross-correlation during the UP state than did the excitation-dominated barrages (both cells held near –75 mV) in the same cells (n = 7 pairs; only UP states were used for the cross-correlation). Cross-correlations between UP states recorded in the same neuron pairs, but randomly shuffled, did not reveal similar correlations (Figures 7C and 7D).

In vivo (Figures 7B, 7E, and 7F), inhibition-dominated barrages were again significantly more synchronized than excitation-dominated barrages (n = 5 pairs), although the cross-correlations for both EPSP- and IPSP-dominated membrane potential traces were lower in vivo than in vitro. Presumably, this lower correlation in vivo results at least in part from the greater average distance between the pairs of recorded cells, since the amplitude of correlation decreases with distance (see below and Supplemental Data). Again, cross-correlations between randomly selected UP states in the neuron pairs (shuffled correlogram) failed to show these large correlations (Figures 7E and 7F).

Examination of the cross-correlations for IPSPs revealed a half-width at half-height of the central peak of 22 ± 4 ms in vitro and 15 ± 7 ms in vivo, while the cross-correlation for EPSPs showed central peaks with a half-width of 24 ± 4 ms in vitro and 19 ± 14 ms in vivo (Figures 7C and 7E). The cross-correlations for IPSPs in vivo often exhibited significant oscillatory components (see Figure 7E) at latencies of 16–25 ms, consistent with the overabundance of gamma frequency oscillations during the generation of UP states in vivo (see Figures 2, 5, and 6). The strength of correlation for both the inhibition- and excitation-dominated barrages decreased strongly with increasing distance between the recorded cells in vivo, ranging from 0.74 (inhibition) and 0.32 (excitation) for a pair that was less than 200 μm apart, to 0.28 and 0.01 for a pair of cells that were approximately 1.2 mm apart. At all distances, the cross-correlation for inhibition-dominated events was higher than that for excitation (see Supplemental Data).

Impact of Synchronized Inhibition on Action Potential Generation

We have seen that inhibitory synaptic barrages received by a neuron during the UP state have more power at frequencies between 2 and 200 Hz and are more synchronized than excitatory synaptic barrages. What are the functional consequences of this difference for action potential timing? To investigate this issue, we used a dynamic-clamp system to inject repeating patterns of excitatory and inhibitory conductances into pyramidal neurons (n = 6). The amplitude and temporal characteristics of the conductance noise were derived from the amplitude and temporal characteris-

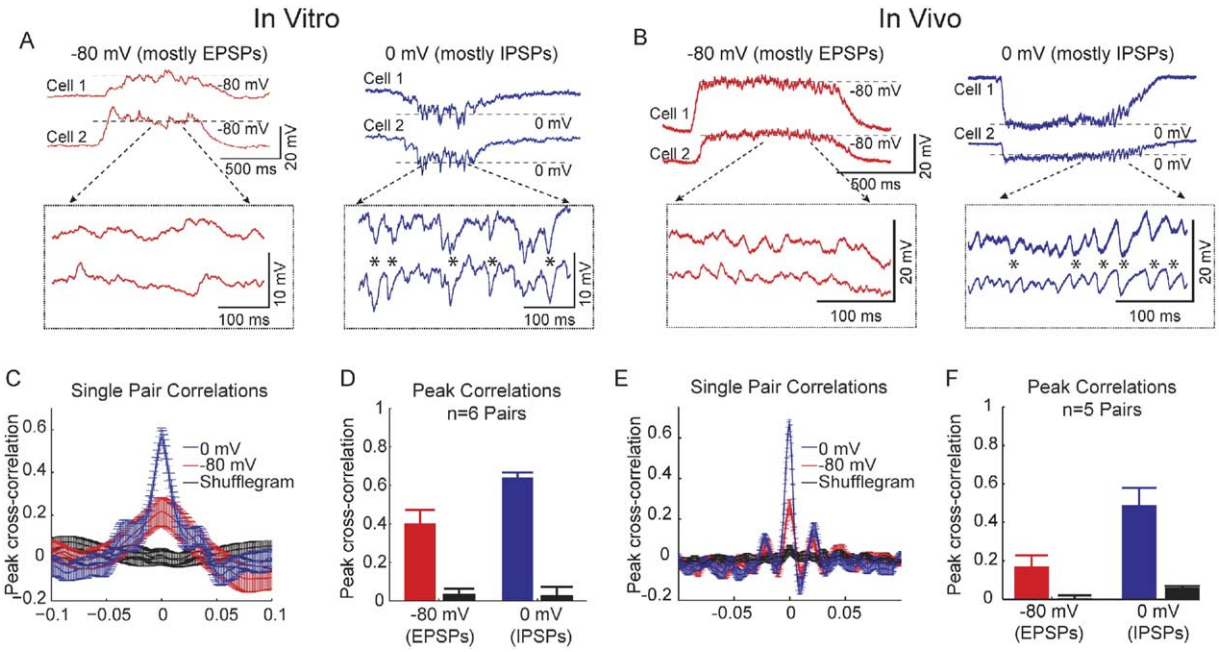

Figure 7. Inhibitory Synaptic Potentials Are More Synchronized Than Excitatory Synaptic Potentials during the Generation of Recurrent Activity In Vitro and In Vivo

(A and B) Simultaneous dual recording of nearby layer 5 pyramidal cells in vitro (A) and in vivo (B). The cells were hyperpolarized (with current) until the UP state was at –80 mV (red) and depolarized until the UP state was at 0 mV (blue). Insets show details of UP states; asterisks show apparently synchronized events. (C and E) Cross-correlations between synaptic potentials at 0 mV (blue) and –80 mV (red), along with shufflegrams (black) for the in vitro (C) and in vivo (E) data; the potentials at 0 mV are significantly more correlated. (D and F) Comparison of cross-correlation peaks at –80 (red, and shufflegram peaks in black) and 0 mV (blue, and shufflegram peaks in black) in n = 6 pairs for in vitro (D) and n = 5 pairs in vivo (F): the potentials at 0 mV are significantly more correlated. Data were collected with sharp electrodes in vivo and in vitro with electrodes containing QX-314 and CsAc. Error bars represent standard error of the mean.

tics of inhibition and excitation in actual UP states recorded in vivo (see Supplemental Data). Just as recorded in vivo, there was an overabundance of power in the 30–80 Hz range (in comparison to the steady falloff of power with frequency), especially in the inhibitory postsynaptic potentials. Repeating epochs of frozen excitatory noise were continuously delivered, while epochs of frozen inhibitory noise alternated with periods of constant inhibitory conductance (Figure 8Aa). The amplitude of the constant inhibitory conductance was equal to the mean of the noisy inhibitory conductance. The duration of the excitatory noise epoch exceeded the duration of the inhibitory noise epoch, so that on each repetition, a given feature of the inhibitory conductance noise would coincide with a different feature of the excitatory conductance noise. Under these conditions, the cell exhibited transient depolarizations in response to either increases in the excitatory noise, decreases in the inhibitory noise, or both (Figure 8Ac).

The recording was divided into periods where inhibitory variance was either present or not, and spike peristimulus time histograms (PSTHs) were constructed, synchronized either on the start of the excitatory or inhibitory frozen noise from periods with and without inhibitory variance. The relationship between PSTH and input conductance could then be quantified, allowing us to calculate how strongly the spike output was modulated by the driving inhibitory and excitatory conductances. Comparing PSTHs synchronized on the beginning of the excitatory conductance constructed from periods with and without variance in the inhibitory conductance reveals the effect of additional noise (variance) on the cell's response to a repeating fluctuating conductance (cf. Figures 8Ba and 8Bb); comparing PSTHs synchronized on the beginning of the excitatory noise (from periods of time with excitatory noise) with PSTHs synchronized on the beginning of the inhibitory noise (from the same periods of time) reveals the differential abilities of realistic inhibition and excitation to modulate action potential generation (cf. Figures 8Bb and 8Bc).

The addition of noise in the inhibitory conductance increased the average peak correlation of the output PSTH with the input excitatory conductance, from 0.27 ± 0.04 to 0.40 ± 0.04 ($p < 0.05$; n = 6 cells) and increased the number of spikes generated during a presentation of the excitatory noise (see Figure 8Ab; increase of 222% ± 58%; n = 6 cells). Controlling for the increase in number of spikes (by resampling the data to contain the same number of action potentials) revealed that the peak correlation in the presence of inhibitory noise remained significantly enhanced, although this effect was much reduced (0.26 ± 0.03 without noise, 0.31 ± 0.04 with noise; n = 6 cells; $p < 0.05$). This result indicates that introduction of variance in the inhibitory conductance increased the correlation between the excitatory

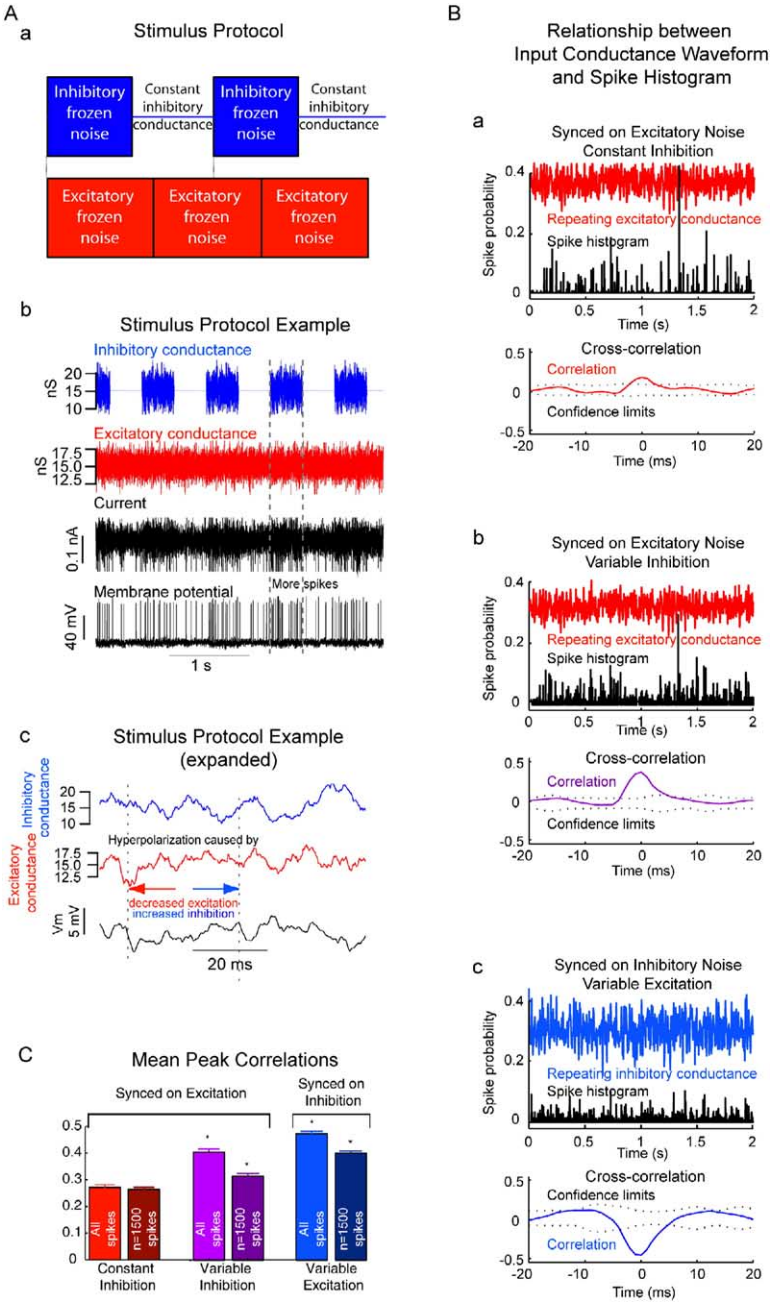

Figure 8. Naturalistic IPSPs Modulate Spike Timing

(A) Phase-shifting injection of frozen excitatory and inhibitory (matched in amplitude and spectral properties to naturally occurring UP states) conductances into a pyramidal cell. (Aa) Stimulus protocol: repeating blocks of excitatory noise are presented simultaneously with alternating blocks of frozen inhibitory noise and constant inhibitory conductance. The durations of the excitatory and inhibitory noise patterns are slightly different, so each presentation of the inhibitory noise begins at a different phase of the excitatory noise. (Ab) Example of recorded data: 2000 ms blocks of repeating inhibition alternated with 2000 ms blocks of constant inhibition of the same average amplitude; inhibition was presented simultaneously with 2014 ms blocks of repeating excitation. At least 200 trials were delivered, so that the excitatory and inhibitory conductances would be presented at all relative phases. (Ac) Expansion of recorded data. (B) Relationship between injected conductances and spike histogram. (Ba) PSTH of spikes generated during periods of constant inhibitory conductance, synced on the start of the excitatory frozen noise (overlaid in red); the cell spiked reliably in discrete events, but the PSTH was poorly correlated with the stimulus waveform. (Bb) PSTH of spikes generated during periods of variable inhibitory conductance, synced on the start of the excitatory frozen noise; the cell no longer spikes in reliable events, but the output PSTH is better correlated with the input conductance. (Bc) PSTH of spikes generated during periods of variable inhibitory conductance, synced on the start of the inhibitory noise. The output PSTH is better correlated with the inhibitory conductance. (C) Group data for n = 6 cells. Adding inhibitory noise increases the number of spikes generated during a presentation of the excitatory noise; whether all spikes are used, or whether a fixed number of spikes are used to calculate the correlation, the presence of variable inhibition increases the correlation of the PSTH with the excitatory conductance input. Analyzing only periods with variable inhibitory conductance, we see that the inhibitory conductance is better represented by the output PSTH than the excitatory conductance is, whether all spikes or a limited number of spikes are used. Data were collected in layer 5 RS cells in a submerged slice with whole-cell patch-clamp recordings. Error bars represent standard error of the mean.

conductance and discharge histogram largely through increasing the number of spikes generated, with a smaller effect of noise alone.

Comparing the effectiveness of excitatory and inhibitory noise in modulating spike output (Figures 8Bb and 8Bc), we see that spiking was better correlated with a reduction of the inhibitory conductance than with an increase in the excitatory conductance: the average peak correlation between the inhibition-synced PSTH and the injected inhibitory conductance was 0.47 ± 0.03, compared to an average peak correlation of 0.40 ± 0.04 between the excitation-synced PSTH and the excitatory conductance (Figure 8C; $p < 0.05$; $n = 6$ cells). Similarly, spike-triggered average of the excitatory and inhibitory conductance revealed a significant increase in g_e (0.55 ± 0.11 nS; $n = 6$ cells) and decrease in g_i (0.89 ± 0.15 nS) just prior to spike initiation (see Supplemental Data). We conclude that naturalistic inhibition is at least as powerful as naturalistic excitation in determining spiking probability and timing.

Discussion

Cortical networks operate through a balance, or proportionality, of recurrent excitation and inhibition, as often revealed by studies examining the synaptic events underlying responses to sensory stimuli (Fregnac et al., 2003; Wehr and Zador, 2003) as well as those mediating spontaneously generated rhythms, such as the UP and DOWN states of the cortical slow oscillation (Shu et al., 2003b). This proportionality of cortical recurrent excitation and inhibition is consistent with the massive recurrent connectivity of the cortex in which excitatory feedback innervates both excitatory (e.g., pyramidal), and local inhibitory neurons and networks.

Signaling within the cerebral cortex involves both the average rate of action potential discharge (e.g., rate code) as well as precise action potential timing (temporal code) (see Lu et al., 2001; Shadlen and Newsome, 1998; Singer, 1999). The ability to generate precise spike times, with millisecond or less resolution, depends upon the generation of higher-frequency fluctuations in the membrane potential (Mainen and Sejnowski, 1995; Nowak et al., 1997). Indeed, the activation of cortical neurons, either by sensory stimuli (reviewed by Singer and Gray, 1995), or during spontaneous UP and DOWN states, is associated with increased power at higher frequencies, particularly in the gamma band (30–80 Hz) (Cowan and Wilson, 1994; Destexhe et al., 1999). Cortical responses can be viewed as having roughly two parts—a low-frequency component that determines the temporally broad excitability of the cell, and a higher-frequency component that determines exactly when action potentials are generated (see Elhilali et al., 2004). Previously, we have shown that the activation of recurrent networks within the cerebral cortex exhibit a maintained depolarization through a balanced increase in activity of recurrent excitatory and inhibitory networks, in which the inhibition and excitation reaching the pyramidal cell on average are approximately equal (Shu et al., 2003b). During spontaneous activity generation of the UP state, this balance of excitation and inhibition interacts with intrinsic inward and outward currents to generate a semistable membrane potential that is near firing threshold (e.g., –60 to –55 mV). Superimposed upon this maintained depolarization are membrane potential fluctuations generated by variations in synaptic barrages. Our results show, after taking into account the differences in driving force on EPSPs and IPSPs at these membrane potentials, that these higher-frequency fluctuations are dominated (by a factor of 1.5–7) by the inhibitory system at frequencies between approximately 2 and 100 Hz. These two findings place the inhibitory networks in a position central to controlling not only the amplitude, extent, and duration of activation of recurrent excitatory cortical networks, but also the precise timing of action potentials and thus, network synchronization (see also Buzsaki and Chrobak, 1995; Csicsvari et al., 2003; Jonas et al., 2004; Jones et al., 2000).

Of the inhibitory networks within the neocortex, those associated with the physiologically defined subclass of FS interneurons seem particularly well tuned to convey broadband frequencies to their postsynaptic targets. Neocortical FS neurons are capable of generating action potentials at a wide range of frequencies with little spike frequency adaptation (McCormick et al., 1985; Nowak et al., 2003). The response of their membrane to the injection of broad band fluctuations shows less decrement of higher frequencies in comparison to RS pyramidal cells (Figure 4) (Fellous et al., 2001), a fact that most likely results in part from the shorter membrane time constant of FS neurons (McCormick et al., 1985; Nowak et al., 2003) and the dominance of K^+ currents near firing threshold in these cells (Fricker and Miles, 2000). FS inhibitory neurons are more able to maintain synaptic transmission at higher frequencies than RS pyramidal cells (Galarreta and Hestrin, 1998; Varela et al., 1999), and they receive kinetically faster EPSPs from presynaptic excitatory cells (Gao and Goldman-Rakic, 2003; Thomson et al., 2002). Many FS neurons preferentially innervate the soma, axon initial segment, and proximal dendritic portions of pyramidal cells, giving them an anatomically preferred placement for the control of spike timing in the postsynaptic neuron (Kawaguchi and Kubota, 1998; Miles et al., 1996; Somogyi et al., 1998; Tamas et al., 1997). Finally, neocortical FS neurons in vivo discharge with a wide range of frequencies and are characterized by a marked sensitivity to the activation of afferent inputs (Jones et al., 2000; Swadlow, 2003; Swadlow et al., 1998). Together, these results indicate that a major component of the cortical inhibitory system, the FS network, is likely to be responsible for conveying broad band frequency fluctuations throughout the network (see also Buzsaki and Chrobak, 1995; Csicsvari et al., 2003; Jefferys et al., 1996; Mann et al., 2005; Penttonen et al., 1998), although an important contribution from non-FS interneurons cannot be excluded (Deans et al., 2001; Mann et al., 2005; Somogyi and Klausberger, 2005).

Our intracellular recordings from the somatic compartment of pyramidal cells during spontaneous UP states in vivo and in vitro revealed that not only did the inhibitory system exhibit more power at frequencies from 2 to 100 Hz than did the recurrent excitatory network, but also that these IPSPs were more synchronized in neighboring (within 1 mm) pyramidal cells. These synchronized IPSPs were often large in amplitude (>5 mV at 10 to –10 mV) and occurred in every recorded pair (n = 6 in vitro and n = 5 in vivo). Although it is possible that a portion of the high correlation between inhibition arriving in nearby pyramidal cells results from a divergent axon from the same presynaptic inhibitory cell, this is unlikely to be the main factor. First, a high correlation was found between the inhibition-dominated PSPs in all eleven pairs of excitatory cells, even though these cells were up to 1.2 mm apart and may have been in different cortical layers. Second, the amplitudes of the IPSP-like events were often larger than expected for unitary IPSPs (Tamas et al., 1997; Tarczy-Hornoch et al., 1998; Thomson et al., 2002). We hypothesize that the high correlation in inhibitory inputs in nearby pyramidal cells results from synchronized activity in the presynaptic GABAergic neurons, generated either through synchronized excitation of these cells by a subset of cells (e.g., chattering cells), or, perhaps more likely, through the cumulative influence of gap

junctions or axonal interconnections between the GABAergic cells of the same inhibitory network (Csicsvari et al., 2003; Galarreta and Hestrin, 1999; Galarreta and Hestrin, 2002; Gibson et al., 1999; Hormuzdi et al., 2001).

In comparison to the activity in excitation-dominated PSPs, the inhibition-dominated PSPs exhibited more power in frequencies from 20 to 100 Hz, often peaking in the gamma frequency range of 30–80 Hz. This finding suggests that the inhibitory networks may be particularly important in the generation and dissemination of gamma frequency activity in cortical networks, as has been previously suggested for the operation of hippocampal networks (see Csicsvari et al., 2003; Jefferys et al., 1996; Mann et al., 2005; Penttonen et al., 1998; Traub et al., 2004). Previously, it has been suggested that a physiologically specialized subclass of pyramidal cells, the chattering cells, are critical to the generation of 30–80 Hz oscillations within cortical networks (Cunningham et al., 2004; Gray and McCormick, 1996). Our results are consistent with this model of high-frequency generation: we hypothesize that, although a portion of the FS cortical inhibitory system may have a propensity to generate synchronized higher-frequency activity in local networks (e.g., Figure 4F), this activity may be driven or enhanced through interactions with networks of excitatory chattering cells, which exhibit a marked intrinsic ability to generate higher-frequency oscillations (Gray and McCormick, 1996).

Previous studies have suggested that the activation of inhibitory networks may provide higher-frequency components by rapidly inhibiting and terminating barrages of excitation arriving in the local network (Pouille and Scanziani, 2001; Wehr and Zador, 2003). Our results extend these prior findings by demonstrating that the proposed importance of inhibitory networks is not limited to initial barrages of excitation in response to a rapid onset event (e.g., rapid and synchronized activation of afferent inputs). Rather, our recordings indicate that the inhibitory PSPs are important to the generation of higher-frequency components of maintained network activity, such as that expected to occur in awake, behaving animals (see Csicsvari et al., 2003).

Through the injection of excitatory and inhibitory conductances that exhibit statistical properties similar to that observed during spontaneous UP states, we were able to demonstrate that action potentials are often generated in response to either a rapid increase in excitation, a rapid decrease in inhibition (Figure 8), or, preferentially, a simultaneous increase in excitation and decrease in inhibition (see Supplemental Data). Through the synchronized control of spike probability and timing in subgroups of pyramidal cells, local inhibitory systems may potently influence diverse cortical functions from gain control to spike timing-dependent synaptic plasticity (Chance et al., 2002; Marder and Buonomano, 2004; Shu et al., 2003a). We hypothesize that the synchronized inhibition of subgroups of neurons is a flexible and dynamically important mode through which the flow of cortical activity is controlled in both space and time. The degree of synchronization determines the amplitude of temporal summation in postsynaptic elements, with greater synchrony driving postsynaptic neurons more effectively. By dynamically synchronizing the discharge of postsynaptic targets, inhibitory networks will potently control the flow of activity and information within the neocortex. This dynamic coupling of varying cortical regions is arguably one of the fundamental features of cortical function—allowing the sheet-like structure of the neocortex to generate, through flexible and rapid associations and dissociations of functional subgroups of cells, the broad range of neuronal assemblies that underlie behavior.

Experimental Procedures

In Vitro Experiments: Interface Chamber

In vitro experiments were performed in layer 5 of slices obtained from the prefrontal cortex anterior to the presylvian sulcus of young (2- to 4-month-old) ferrets. Slices were cut on a DSK microslicer (Ted Pella Inc., Redding, CA) or a Leica Vibratome in a slice solution in which the NaCl was replaced with sucrose. The slices (0.4 mm thick) were maintained in an interface-style recording chamber at 35°C–36°C in a solution containing 126 mM NaCl, 2.5 mM KCl, 2 mM $MgSO_4$, 1.25 mM NaH_2PO4, 2 mM $CaCl_2$, 26 mM $NaHCO_3$, and 10 mM dextrose, and aerated with 95% O_2, 5% CO_2 to a final pH of 7.4. After approximately 1 hr, the slice solution was modified to contain 1 mM $MgSO_4$, 1 mM $CaCl_2$, and 3.5 mM KCl. Simultaneous extracellular multiple-unit and intracellular recordings were performed in layer 5 following 2 hr of recovery.

In Vitro Experiments: Submerged Slices

Slices (0.3 mm thick) maintained in submerged chambers (at 35.5°C) were incubated at 35°C for 45 min, then maintained at room temperature until use. Incubation and slice solution contained 125 mM NaCl, 2.5 mM KCl, 1 mM $MgCl_2$, 1.25 mM NaH_2PO_4, 2 mM $CaCl_2$, 25 mM $NaHCO_3$, and 25 mM dextrose, aerated with 95% O_2, 5% CO_2 to a final pH of 7.4. This solution was used for the investigation of cellular properties of RS and FS neurons in layer 5 of prefrontal cortex, since in this medium, slices are quiescent, and no network activity interferes with the observation of intrinsic membrane properties.

In Vivo Experiments

Two- to four-month-old male ferrets were anesthetized with ketamine (30 mg/kg i.m.) and xylazine (1 mg/kg i.m.) and mounted in a stereotaxic frame. In order to minimize pulsation arising from the heartbeat and respiration, a cisternal drainage was performed. During recording, anesthesia was maintained with intramuscular supplemental doses of ketamine/xylazine. The heart rate and rectal temperature were monitored throughout the experiment and maintained at 160–210 bpm and 37°C–38°C, respectively. The EEG and the absence of reaction to noxious stimuli were regularly checked. After the recording session, the animal was given a lethal injection of sodium pentobarbital. All protocols were approved by the Yale University Institutional Animal Care and Use Committee and conformed to the guidelines recommended in "Preparation and Maintenance of Higher Mammals During Neuroscience Experiments" (NIH publication No. 91-3207).

Extra- and intracellular recordings were performed in the prefrontal cortex anterior to the presylvian sulcus. The extracellular broadband, multiple-unit, gamma band, and field recordings were obtained from the same tungsten microelectrode (<0.5 MΩ, multiple-unit; 1–5 MΩ, single-unit) lowered into either the supra- or infragranular layers; traces marked "Extracellular" were obtained by band-pass filtering the recording from the tungsten microelectrode at 0.1–20 kHz, while traces marked "30–80 Hz" were obtained by filtering the recording from the tungsten microelectrode at 30-80 Hz. Local field potential recordings (not shown) were obtained by low-pass filtering the recording at 100 Hz, and multiple-unit recordings (not shown) were obtained by band-pass filtering the recording at 300–20 kHz. Intracellular recordings were then obtained from a sharp glass microelectrode positioned within 0.5 mm of the entry point of the extracellular recording electrode. Following positioning of the intracellular electrode, the opening in the skull was sealed with agar (4% in saline). Paired intracellular sharp electrode record-

ings were performed with the entry point of the microelectrodes within 1200 μm in vivo and typically within 100 μm in vitro. Absolute distances between recorded cells were estimated by using the linear distance indicated on the manipulators and the angle of the electrode placement, and by stereotaxic measurement of the points of entry into the cortex.

Electrophysiological Recordings

Whole-Cell Patch Recordings

Intracellular whole-cell recordings were obtained with glass pipettes pulled on a P-97 micropipette puller (Sutter Instruments, Novato, CA) from 1BF-200 glass (WPI, Sarasota, FL) to 2.5–3 MΩ and fire polished using a Narishige microforge and filled with 163 mM KMe SO_4, 2 mM $MgCl_2$, 2 mM Na_2ATP, 10 mM HEPES, and 0.2 mM EGTA, and having a pH of 7.3. Intracellular signals were amplified with an Axopatch-200B or Axopatch-1D amplifier (Axon Instruments, Foster City, CA) in either current- or voltage-clamp mode.

Sharp Electrode Recordings

Intracellular recordings were performed using conventional sharp electrodes, pulled on a P-80 micropipette puller (Sutter Instruments, Novato, CA) from medium-walled glass capillaries (1BF100, WPI, Sarasota, FL) and beveled to resistances of 60–90 MΩ, and that either contained 50 mM QX-314 and 2 M CsAc, which blocks voltage-dependent Na^+ currents and reduces K^+ currents (including the h-current) and $GABA_B$-mediated synaptic potentials, or 2 M KAc. Intracellular signals were amplified with an Axoclamp-2B amplifier (Axon Instruments, Foster City, CA) in either current-clamp or single-electrode voltage-clamp mode.

Previously, we have shown that the single-electrode voltage clamp through a sharp microelectrode is sufficient to accurately determine the reversal potential of EPSPs and IPSPs of widely varying amplitudes (see supplementary material for Shu et al., 2003b). Excitatory postsynaptic potentials in vitro, with the methods used here, were found to reverse near 0 mV, while inhibitory postsynaptic potentials in vitro reversed near –80 mV. Therefore, to maximize the contribution of excitatory conductances (and minimize the contribution of inhibitory conductances), we examine EPSPs/EPSCs at –80 ± 5 mV. Likewise, to maximize the contributions of inhibitory conductances and minimize the contribution of excitatory conductances, we examine IPSPs/IPSCs at a membrane potential of 0 ± 5 mV. Note that, in current-clamp recordings, we inject current so that the membrane potential of the UP state is at the target potential (see Figure 2A), while in voltage-clamp recordings, the holding potential is the target potential (see Figure 1B). Although these recordings will not perfectly separate excitatory and inhibitory components of the UP state, they will result in large differences in the contributions of excitation and inhibition to the measured voltage or current fluctuations. These differences are the subject of this study.

In all experimental conditions, intracellular recordings were accepted if they showed a stable membrane potential below –55 mV at rest and an input resistance larger than 20 MΩ. In both sharp electrode and whole-cell patch-clamp recordings, only data collected from RS and FS neurons were included for analysis. The recorded signals were acquired, digitized, and analyzed with Spike2 system and software (CED, Cambridge, UK).

Detection of UP and DOWN States

Because intracellularly recorded UP and DOWN states have very different characteristics at different membrane potentials, extracellular multiple-unit recordings were used to determine the times at which UP and DOWN states began and ended. To detect the onset of the UP state, the multiple-unit recording was rectified and smoothed to yield an outline of the increase and decrease in activity associated with the onset and offset of the UP state. Two thresholds were set, and the multiple-unit activity was required to rise above the highest threshold to be counted as an UP state. The onset and offset of the UP state were then determined by the crossings of the lower threshold, which was set at approximately 2× baseline. Only UP states that were at least 0.3 s in duration and DOWN states that were at least 0.1 s in duration were considered.

Characterization of Physiological Cell Type

Of the four broad electrophysiological classes of cortical neurons consistently recorded in vivo (Nowak et al., 2003), we concentrated our present study on the RS and FS categories. RS neurons are the most commonly recorded cell type and are characterized by broader action potentials, spike frequency adaptation, and a relatively shallow f-I relation. Our intracellular morphological analyses have revealed that with sharp intracellular electrodes RS neurons are invariably pyramidal cells (McCormick et al., 1985; Nowak et al., 2003). In our whole-cell recordings in vitro, RS cells exhibited pyramidal-shaped cell bodies under DIC imaging. However, it is at least theoretically possible, but highly unlikely, that our sample of RS cells includes one or more nonpyramidal neurons (Markram et al., 2004).

FS neurons are characterized by relatively brief duration action potentials, a relative lack of spike frequency adaptation, and a steep f-I relation. Electrophysiologically identified FS neurons are GABAergic inhibitory cells (McCormick et al., 1985; Nowak et al., 2003).

Extracellularly recorded single units were classified based on two criteria: spike duration (from first deviation away from baseline, past the spike peak and trough, to 2/3 repolarization) and the ratio of the spike peak height to trough depth. When recorded extracellularly, FS interneuron action potentials are typically brief (<1 ms), and have troughs that are deep relative to their peaks (indicating rapid membrane repolarization), while RS action potentials are typically longer (1–3 ms) and have troughs that are shallow relative to their peaks (indicating slower membrane repolarization) (Csicsvari et al., 1999; McCormick et al., 1985). The combination of these two criteria sufficed to clearly distinguish RS from FS spikes (Figure S3).

Mathematical Methods

A full description of the mathematical methods is given in the Supplemental Data. Power spectra were calculated using Welch's method. Continuous transfer functions were estimated using Welch's averaged periodogram method. Discrete transfer functions were estimated using Wiener's method. All error bars were calculated as the standard error of the mean.

A number of experiments were performed with a dynamic-clamp technique using a DAP-5216a board (Microstar Laboratory). Noisy conductances were constructed according to an Ornstein-Uhlenbeck (colored noise) model. For measurement of subthreshold transfer function, a cell was placed at its resting potential; a conductance with reversal potential of 0 mV and a time constant of 5 ms, and whose standard deviation was half its mean, was injected into the cell. The standard deviation (and, concurrently, the amplitude) of the conductance was adjusted to give a 10 mV peak-to-peak membrane potential deviation, and the holding current was adjusted to keep the cell just below spike threshold. Transfer function from the injected conductance to the recorded membrane potential fluctuations was then calculated. For measurement of suprathreshold transfer function, the cell was then depolarized to give a mean spike rate of 5 Hz, and the transfer between the injected conductance and the spike times was calculated. For mimicking natural recurrent activity, two dynamic-clamp systems were used in parallel: one generated a conductance with a reversal potential of 0 mV (mimicking excitation), and the other generated a conductance with a reversal potential of –80 mV (mimicking inhibition). Inhibitory and excitatory conductance patterns were constructed, starting from naturally occurring (DC-removed) IPSP and EPSP barrages in vivo (see Supplemental Data).

Supplemental Data

The Supplemental Data include Experimental Procedures and seven figures and can be found with this article online at http://www.neuron.org/cgi/content/full/47/3/423/DC1/.

Acknowledgments

This work was supported by the National Institutes of Health (D.A.M.), the Howard Hughes Institute (A.H.), the Beinecke Foundation (A.H.), Pfizer Corp. (B.H.), and the Kavli Institute for Neuroscience.

Received: December 20, 2004
Revised: April 25, 2005
Accepted: June 15, 2005
Published: August 3, 2005

References

Buzsaki, G., and Chrobak, J.J. (1995). Temporal structure in spatially organized neuronal ensembles: a role for interneuronal networks. Curr. Opin. Neurobiol. *5*, 504–510.

Buzsaki, G., and Draguhn, A. (2004). Neuronal oscillations in cortical networks. Science *304*, 1926–1929.

Chance, F.S., Abbott, L.F., and Reyes, A.D. (2002). Gain modulation from background synaptic input. Neuron *35*, 773–782.

Cobb, S.R., Buhl, E.H., Halasy, K., Paulsen, O., and Somogyi, P. (1995). Synchronization of neuronal activity in hippocampus by individual GABAergic interneurons. Nature *378*, 75–78.

Cowan, R.L., and Wilson, C.J. (1994). Spontaneous firing patterns and axonal projections of single corticostriatal neurons in the rat medial agranular cortex. J. Neurophysiol. *71*, 17–32.

Csicsvari, J., Hirase, H., Czurko, A., Mamiya, A., and Buzsaki, G. (1999). Oscillatory coupling of hippocampal pyramidal cells and interneurons in the behaving rat. J. Neurosci. *19*, 274–287.

Csicsvari, J., Jamieson, B., Wise, K.D., and Buzsaki, G. (2003). Mechanisms of gamma oscillations in the hippocampus of the behaving rat. Neuron *37*, 311–322.

Cunningham, M.O., Whittington, M.A., Bibbig, A., Roopun, A., LeBeau, F.E., Vogt, A., Monyer, H., Buhl, E.H., and Traub, R.D. (2004). A role for fast rhythmic bursting neurons in cortical gamma oscillations in vitro. Proc. Natl. Acad. Sci. USA *101*, 7152–7157.

Deans, M.R., Gibson, J.R., Sellitto, C., Connors, B.W., and Paul, D.L. (2001). Synchronous activity of inhibitory networks in neocortex requires electrical synapses containing connexin36. Neuron *31*, 477–485.

Destexhe, A., Contreras, D., and Steriade, M. (1999). Spatiotemporal analysis of local field potentials and unit discharges in cat cerebral cortex during natural wake and sleep states. J. Neurosci. *19*, 4595–4608.

Elhilali, M., Fritz, J.B., Klein, D.J., Simon, J.Z., and Shamma, S.A. (2004). Dynamics of precise spike timing in primary auditory cortex. J. Neurosci. *24*, 1159–1172.

Fellous, J.M., Houweling, A.R., Modi, R.H., Rao, R.P., Tiesinga, P.H., and Sejnowski, T.J. (2001). Frequency dependence of spike timing reliability in cortical pyramidal cells and interneurons. J. Neurophysiol. *85*, 1782–1787.

Foffani, G., Tutunculer, B., and Moxon, K.A. (2004). Role of spike timing in the forelimb somatosensory cortex of the rat. J. Neurosci. *24*, 7266–7271.

Fregnac, Y., Monier, C., Chavane, F., Baudot, P., and Graham, L. (2003). Shunting inhibition, a silent step in visual cortical computation. J. Physiol. (Paris) *97*, 441–451.

Fricker, D., and Miles, R. (2000). EPSP amplification and the precision of spike timing in hippocampal neurons. Neuron *28*, 559–569.

Galarreta, M., and Hestrin, S. (1998). Frequency-dependent synaptic depression and the balance of excitation and inhibition in the neocortex. Nat. Neurosci. *1*, 587–594.

Galarreta, M., and Hestrin, S. (1999). A network of fast-spiking cells in the neocortex connected by electrical synapses. Nature *402*, 72–75.

Galarreta, M., and Hestrin, S. (2002). Electrical and chemical synapses among parvalbumin fast-spiking GABAergic interneurons in adult mouse neocortex. Proc. Natl. Acad. Sci. USA *99*, 12438–12443.

Gao, W.J., and Goldman-Rakic, P.S. (2003). Selective modulation of excitatory and inhibitory microcircuits by dopamine. Proc. Natl. Acad. Sci. USA *100*, 2836–2841.

Gibson, J.R., Beierlein, M., and Connors, B.W. (1999). Two networks of electrically coupled inhibitory neurons in neocortex. Nature *402*, 75–79.

Gibson, J.R., Beierlein, M., and Connors, B.W. (2005). Functional properties of electrical synapses between inhibitory interneurons of neocortical layer 4. J. Neurophysiol. *93*, 467–480.

Gray, C.M., and McCormick, D.A. (1996). Chattering cells: superficial pyramidal neurons contributing to the generation of synchronous oscillations in the visual cortex. Science *274*, 109–113.

Hormuzdi, S.G., Pais, I., LeBeau, F.E., Towers, S.K., Rozov, A., Buhl, E.H., Whittington, M.A., and Monyer, H. (2001). Impaired electrical signaling disrupts gamma frequency oscillations in connexin 36-deficient mice. Neuron *31*, 487–495.

Jefferys, J.G., Traub, R.D., and Whittington, M.A. (1996). Neuronal networks for induced '40 Hz' rhythms. Trends Neurosci. *19*, 202–208.

Jonas, P., Bischofberger, J., Fricker, D., and Miles, R. (2004). Interneuron Diversity series: Fast in, fast out—temporal and spatial signal processing in hippocampal interneurons. Trends Neurosci. *27*, 30–40.

Jones, M.S., MacDonald, K.D., Choi, B., Dudek, F.E., and Barth, D.S. (2000). Intracellular correlates of fast (>200 Hz) electrical oscillations in rat somatosensory cortex. J. Neurophysiol. *84*, 1505–1518.

Kawaguchi, Y. (1995). Physiological subgroups of nonpyramidal cells with specific morphological characteristics in layer II/III of rat frontal cortex. J. Neurosci. *15*, 2638–2655.

Kawaguchi, Y., and Kubota, Y. (1998). Neurochemical features and synaptic connections of large physiologically-identified GABAergic cells in the rat frontal cortex. Neuroscience *85*, 677–701.

Lu, T., Liang, L., and Wang, X. (2001). Temporal and rate representations of time-varying signals in the auditory cortex of awake primates. Nat. Neurosci. *4*, 1131–1138.

Mainen, Z.F., and Sejnowski, T.J. (1995). Reliability of spike timing in neocortical neurons. Science *268*, 1503–1506.

Mann, E.O., Radcliffe, C.A., and Paulsen, O. (2005). Hippocampal gamma-frequency oscillations: from interneurones to pyramidal cells, and back. J. Physiol. *562*, 55–63.

Marder, C.P., and Buonomano, D.V. (2004). Timing and balance of inhibition enhance the effect of long-term potentiation on cell firing. J. Neurosci. *24*, 8873–8884.

Markram, H., Toledo-Rodriguez, M., Wang, Y., Gupta, A., Silberberg, G., and Wu, C. (2004). Interneurons of the neocortical inhibitory system. Nat. Rev. Neurosci. *5*, 793–807.

McCormick, D.A., Connors, B.W., Lighthall, J.W., and Prince, D.A. (1985). Comparative electrophysiology of pyramidal and sparsely spiny stellate neurons of the neocortex. J. Neurophysiol. *54*, 782–806.

Miles, R., Toth, K., Gulyas, A.I., Hajos, N., and Freund, T.F. (1996). Differences between somatic and dendritic inhibition in the hippocampus. Neuron *16*, 815–823.

Nowak, L.G., Sanchez-Vives, M.V., and McCormick, D.A. (1997). Influence of low and high frequency inputs on spike timing in visual cortical neurons. Cereb. Cortex *7*, 487–501.

Nowak, L.G., Azouz, R., Sanchez-Vives, M.V., Gray, C.M., and McCormick, D.A. (2003). Electrophysiological classes of cat primary visual cortical neurons in vivo as revealed by quantitative analyses. J. Neurophysiol. *89*, 1541–1566.

Penttonen, M., Kamondi, A., Acsady, L., and Buzsaki, G. (1998). Gamma frequency oscillation in the hippocampus of the rat: intracellular analysis in vivo. Eur. J. Neurosci. *10*, 718–728.

Pouille, F., and Scanziani, M. (2001). Enforcement of temporal fidelity in pyramidal cells by somatic feed-forward inhibition. Science *293*, 1159–1163.

Sanchez-Vives, M.V., and McCormick, D.A. (2000). Cellular and network mechanisms of rhythmic recurrent activity in neocortex. Nat. Neurosci. *3*, 1027–1034.

Shadlen, M.N., and Newsome, W.T. (1998). The variable discharge of cortical neurons: implications for connectivity, computation, and information coding. J. Neurosci. *18*, 3870–3896.

Shu, Y., Hasenstaub, A., Badoual, M., Bal, T., and McCormick, D.A. (2003a). Barrages of synaptic activity control the gain and sensitivity of cortical neurons. J. Neurosci. *23*, 10388–10401.

Shu, Y., Hasenstaub, A., and McCormick, D.A. (2003b). Turning on and off recurrent balanced cortical activity. Nature *423*, 288–293.

Singer, W. (1999). Time as coding space? Curr. Opin. Neurobiol. *9*, 189–194.

Singer, W., and Gray, C.M. (1995). Visual feature integration and the temporal correlation hypothesis. Annu. Rev. Neurosci. *18*, 555–586.

Somogyi, P., and Klausberger, T. (2005). Defined types of cortical interneurone structure space and spike timing in the hippocampus. J. Physiol. *562*, 9–26.

Somogyi, P., Tamas, G., Lujan, R., and Buhl, E.H. (1998). Salient features of synaptic organisation in the cerebral cortex. Brain Res. Brain Res. Rev. *26*, 113–135.

Steriade, M. (1997). Synchronized activities of coupled oscillators in the cerebral cortex and thalamus at different levels of vigilance. Cereb. Cortex *7*, 583–604.

Steriade, M., McCormick, D.A., and Sejnowski, T.J. (1993a). Thalamocortical oscillations in the sleeping and aroused brain. Science *262*, 679–685.

Steriade, M., Nunez, A., and Amzica, F. (1993b). A novel slow (< 1 Hz) oscillation of neocortical neurons in vivo: depolarizing and hyperpolarizing components. J. Neurosci. *13*, 3252–3265.

Steriade, M., Timofeev, I., and Grenier, F. (2001). Natural waking and sleep states: a view from inside neocortical neurons. J. Neurophysiol. *85*, 1969–1985.

Swadlow, H.A. (2003). Fast-spike interneurons and feedforward inhibition in awake sensory neocortex. Cereb. Cortex *13*, 25–32.

Swadlow, H.A., Beloozerova, I.N., and Sirota, M.G. (1998). Sharp, local synchrony among putative feed-forward inhibitory interneurons of rabbit somatosensory cortex. J. Neurophysiol. *79*, 567–582.

Tamas, G., Buhl, E.H., and Somogyi, P. (1997). Fast IPSPs elicited via multiple synaptic release sites by different types of GABAergic neurone in the cat visual cortex. J. Physiol. *500*, 715–738.

Tarczy-Hornoch, K., Martin, K.A., Jack, J.J., and Stratford, K.J. (1998). Synaptic interactions between smooth and spiny neurones in layer 4 of cat visual cortex in vitro. J. Physiol. *508*, 351–363.

Thomson, A.M., West, D.C., Wang, Y., and Bannister, A.P. (2002). Synaptic connections and small circuits involving excitatory and inhibitory neurons in layers 2–5 of adult rat and cat neocortex: triple intracellular recordings and biocytin labelling in vitro. Cereb. Cortex *12*, 936–953.

Traub, R.D., Bibbig, A., LeBeau, F.E., Buhl, E.H., and Whittington, M.A. (2004). Cellular mechanisms of neuronal population oscillations in the hippocampus in vitro. Annu. Rev. Neurosci. *27*, 247–278.

Varela, J.A., Song, S., Turrigiano, G.G., and Nelson, S.B. (1999). Differential depression at excitatory and inhibitory synapses in visual cortex. J. Neurosci. *19*, 4293–4304.

Wehr, M., and Zador, A.M. (2003). Balanced inhibition underlies tuning and sharpens spike timing in auditory cortex. Nature *426*, 442–446.

Whittington, M.A., Traub, R.D., and Jefferys, J.G. (1995). Synchronized oscillations in interneuron networks driven by metabotropic glutamate receptor activation. Nature *373*, 612–615.